13th International Symposium on Particle Image Velocimetry – ISPIV 2019
Munich, Germany, July 22-24, 2019

Experimental investigation on bubble chains with varying bubble frequencies and narrow size distributions using a Shadow-PIV setup

Stefan Ostmann[1*], Max Finster[1] and Rüdiger Schwarze[1]

[1] TU Bergakademie Freiberg, Institute of Mechanics and Fluid Dynamics, Freiberg, Germany
[*]stefan.ostmann@imfd.tu-freiberg.de

1 Introduction

The investigation of the nature of bubbly flows is a long standing task in the field of numerical as well as in the field of experimental fluid mechanics. The flow is not only influenced on the spatial scale of the bubble itself, but develops helical macro structures, which on their part influence the bubble dynamics forming a complex interacting system. As there are numerous experimental and numerical works on bubbly flows, one of the major issues causing problems regarding the comparison of numerical an experimental results is the lack of carefully defined boundary conditions, see Elghobashi (2019). Additionally, there are hardly any experiments which show combined measurements of the bubble characteristics and their surrounding flow. Although, Sommerfeld and Bröder (2009) showed the interaction of bubbles in dispersed flow through the liquid phase, the information of the developing flow field within dispersed gas/liquid flow is very limited. Especially, the emergence of so called bubble-turbulence is an open question which could only be investigated under carefully chosen boundary conditions. The present study aims to contribute to the field by the analysis of monodispersed bubble chains at various frequencies. The proposed setup allows for the precise conditioning of bubbly flows and also offers good optical accessibility, which at the time offers the opportunity of combined measurements of the dispersed, as well as of the continuous phase.

2 Experimental Setup

The experiments were conducted within a thin bubble column with a 100x30 mm cross section and a height of 300 mm (see figure 1). The fluids in use were tap water and compressed air at ambient conditions. The water was seeded, using Dantec-Polyamide seeding particles ($\rho = 1.03$ g/cm^3, $d_m = 20\ \mu$m).

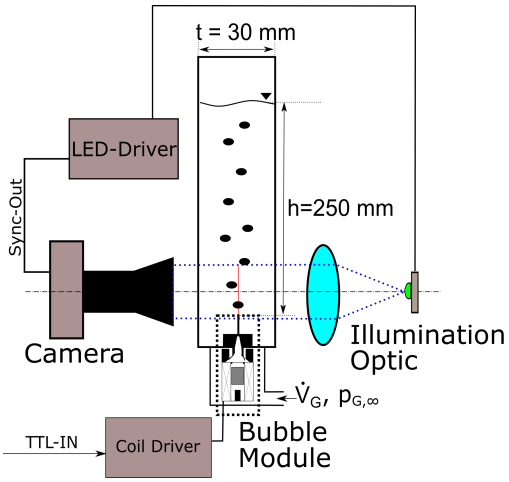

Figure 1: Experimental Setup

The bubbles were injected at the bottom center using a plane metal syringe with an inner diameter of $D = 0.3$ mm. The inner walls of the syringe are coated with paraffin to reduce the wetting angle in a similar way as Vejrazka et al. (2008) to prevent water from entering the gas chamber of the bubbling modules. The syringes outer walls are desired to have a wetting angle as high as possible to ensure that the wetting circle stays fixed to the syringe tip. This condition is ensured by frequent cleaning of the outer capillary walls with ethanol.

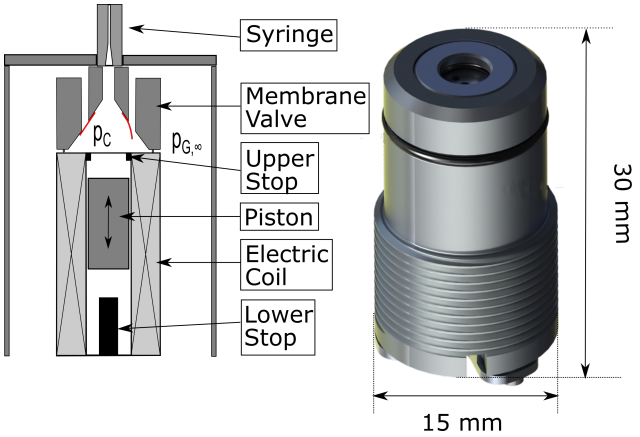

Figure 2: Setup bubble module

The bubble module is supplied with compressed air at a static-over pressure of $p_{G,\infty} = 150$ mPa, which prevents water from entering the prechamber of the modules. The bubbles were produced by an in-house developed module, which is operated by TTL level signals, allowing for a precise specification of the bubble frequency and relatively narrow and bubble size distributions. The bubble modules are set up in a similar way as described in Ostmann and Schwarze (2018). The modules consist of a cylinder-piston system (see figure 2). In unacuated mode the piston rests on the lower stop. If the magnetic piston is actuated by the magnetic coil, that is wrapped around the outer cylinder walls, the cylinder is driven upwards pushing the air, located within the chamber through the syringe, forming a bubble that detaches as soon as the piston reaches the upper stop. At the idle period the piston travels back down onto the lower stop. The arising low pressure triggers the membrane valve and air is flowing back into the chamber. The temporal deviation of the moment of detachment is distributed statistically and lies in the magnitude of $\Delta t_{\mathrm{Det}} = 0.2...0.5$ ms. The power consumption of the modules is in the magnitude of 1 W and the piston stroke in the current experimental setup was set to 1 mm or 1.5 mm, respectively.
For the measurement of the bubble characteristics and the surrounding flow a transmitted-light setup was used. Illumination was provided by a pulsed collimated High Power LED, operated at a pulse length of $\Delta t_{aq} = 5$ μs. For imaging a CMOS high speed camera type Microtron MotionBlitz Mini2 at a resolution of 704x1746 Pixels was used. The temporal resolution was at 1170 fps. The imaging optic was a high-aperture f = 60 mm lens combined with lens converter tubes, resulting in a pixel resolution of 10 μm/Pixel and a field of view of approximately $7x17$ mm. The depth of field was determined experimentally and is below 150 mum and the focal plane was set exactly on the needle tip. The information extraction process is split into two parts. On the one hand side the measurement of the flow field by means of Particle Image Velocimetry and on the other side the determination of the bubble characteristic. For the PIV evaluations the software LaVision Davis 8.4.0 was used. For each experiment a set of 500 images were evaluated. In the first step a mask was defined. The mask is composed of a static part, which could be applied to every image in the series (see figure 3(a), blue area) and a dynamic or algorithmic mask, which adjusts to the present bubbles at every time step (figure 3(a), red area).
On the masked out images the PIV analysis is applied, using the following parameters. The cross correlation is executed as multi-pass correlation with decreasing windows size. Starting at 32x32 Pixels square window size and after that decreasing to a window size of 16x16 Pixels with an adapting weighting function with two passes. The overlap in all correlation steps was set to 50 %. Additionally, outlier vectors were filtered using a median filter with a 5x5 kernel for universal outlier detection. An exemplary vectorfield could be seen in 3(b). It could be seen that within the area of the dynamic mask of the bubbles no velocity vectors could be calculated. However, especially the fluid flow near the bubble surface would be an interesting information, regarding the transfer of the bubbles surface oscillation to the fluid flow. In the final step the velocity field

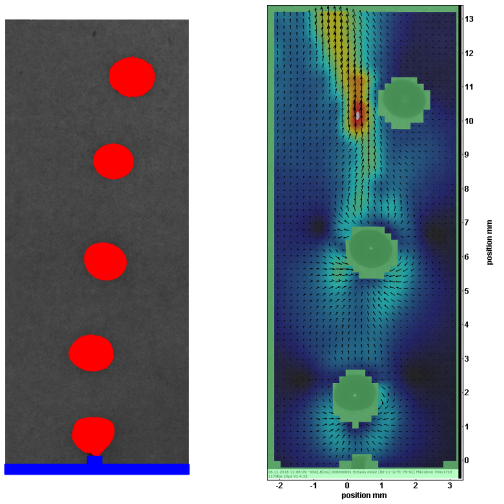

(a) Masked out image (Red Area indicates the dynamic part, blue area the static part)

(b) Raw PIV vector field

Figure 3: Exemplary processing chain for the PIV analysis

was smoothed, applying a Gaussian filter with a 3x3x3 kernel in space and time. Figure 4 shows exemplary PIV correlation coefficients for bubbling frequencies of 20 Hz, as well as 70 Hz (right subimage). It could be seen that the correlation values within the proximity of the bubbles, especially within the vertical spacing between the bubbles tend to reduce drastically to values below 0.5, while being well above 0.8 outside the bubble path. This tendency is dependent on the bubbling frequency, which reflects the evolving three dimensional nature of the flow field developing around the bubble chains. Another explanation could be that high frequency modes of the bubbles surface oscillation decay much more rapidly with distance to the bubble. Figure 5 shows the procedure for the evaluation of the single bubbles. The raw images already show

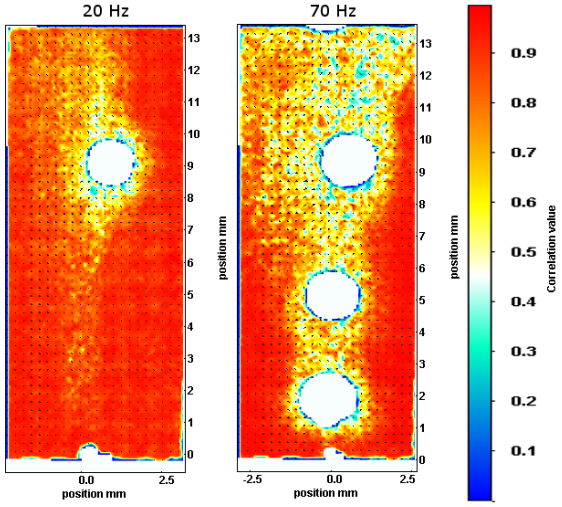

Figure 4: PIV correlation values for bubbling frequencies of 20 (left) and 70 Hz (right)

a clear separation of the bubble phase to the domain of liquid flow, by means of the bubble area the color value. Within the first step the raw image is inverted and the contrast is further enhanced using histogram equalisation. In the next processing step the images are binarised, using a combined threshold and sub-pixel edge-detection based closing. Furthermore, remaining small objects are removed by means of a minimum-area criterion. Using the binary image only containing bubbles, which are clearly separated from each, the

bubbles can now be segmented and each bubble, at each other time step could now be analysed, be means of their centroid position, equivalent diameter and their axis main axis ratio. For the calculation of the volume equivalent diameter the bubbles were assumed to possess rotational symmetry with respect to the symmetry plane.

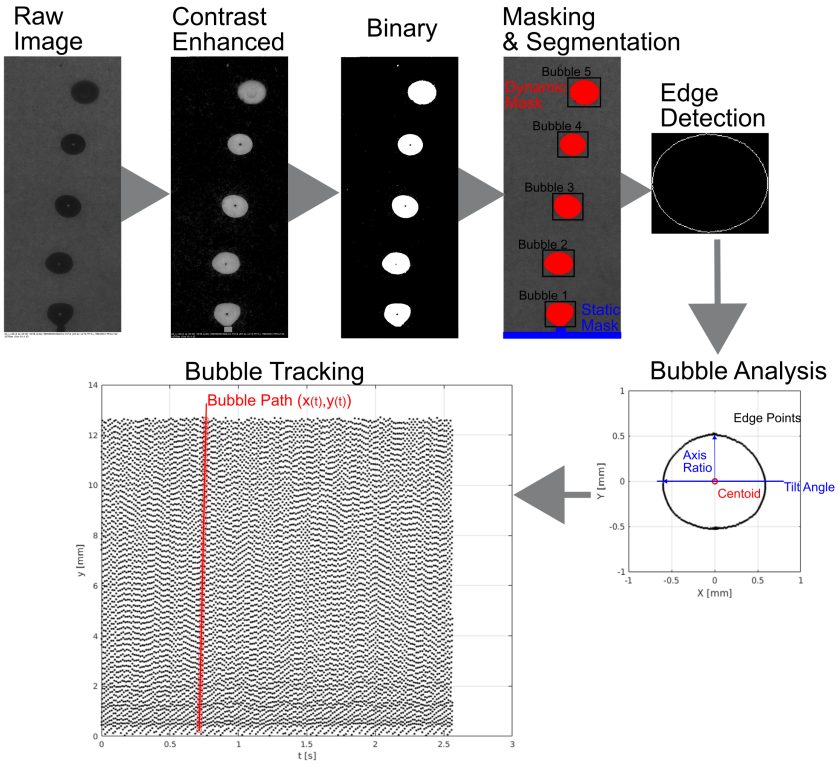

Figure 5: Processing chain for bubble characteristics

The final processing step is the bubble tracking, which is, due to their ascending nature and the absence of overlapping, relatively straight forward. The diagram on the lower part of figure 5 shows a diagram which contains the vertical position of all detected bubbles with respect to the detection frame (time). The bubbles are initialised on their lowest position, and the algorithm tries to find the distinct bubble within the next two time steps by the criteria, that the bubbles equivalent size only chances marginally and their vertical position increases in relation to the origin, which was set to be on the needle tip. This process leads a set of array, whose every element represents the path of one bubble with respect to time, including the position, axis ratio and diameter (indicated by the red markers within the diagram in figure 5). In the final set the bubbles velocity is calculated.

3 Results

Within the present study one set of bubbles was analysed. The bubble diameter was held approximately constant for all bubbling frequencies (see figure 6(a)). The diameter deviation over all measured frequencies is below 5 %, considering the volume equivalent diameter d_m, although the mean diameter is decreasing towards higher frequencies, which might be subjected to the sluggishness of the gas supply system. However the diameter within the frequency measurements are below 1% in relation to the median diameter of the set. Figure 6(b) shows the resulting dimensionless bubble spacing, herein defined as the reciprocal Strouhal number $L^* = Sr^{-1} = u_m / f_{bub} \cdot d_m$. The dataset extends to dimensionless bubble spacings of 12 d_m for 20 Hz to roughly 2.1 d_m at 100 Hz. Any higher frequency for the given bubble diameter resulted in near orifice

coalescence, with the consequence of much broader bubble size distributions and the loss of accurate timing and are therefore not considered in the present report.

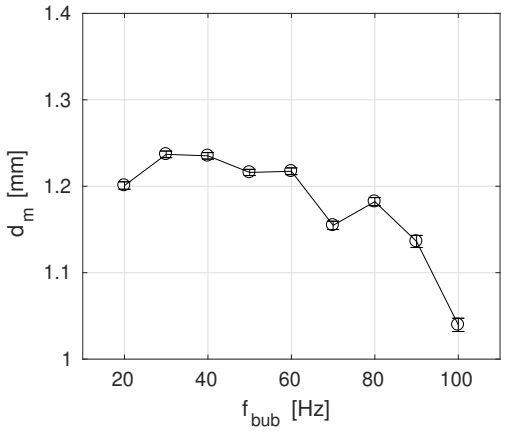

(a) diameter derivations of the investigated bubbles with respect to the bubbling frequency

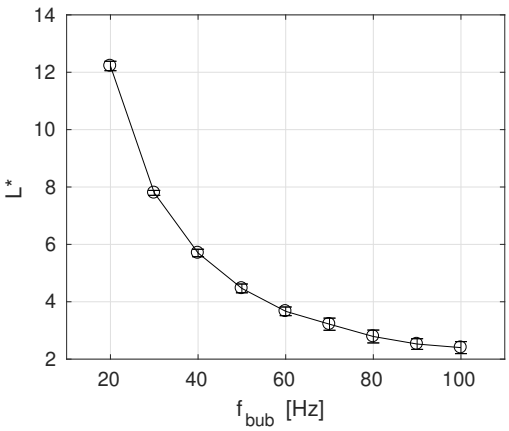

(b) dimensionless bubble spacing (L*) over bubble frequency

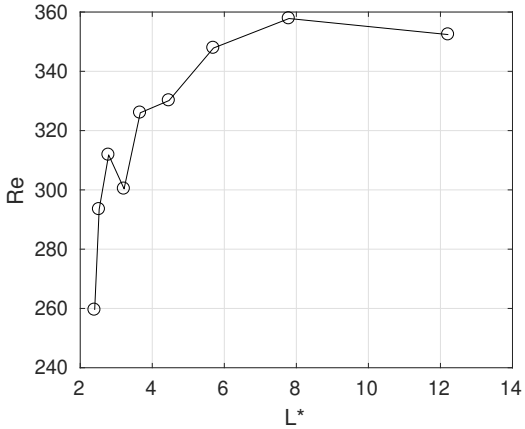

(c) free-stream Reynolds number over dimensionless bubble spacing

Figure 6: General Bubble Characteristics

Figure 6(c) displays the median free stream Reynolds numbers in relation to the dimensionless bubble spacing. Herein the Reynolds numbers were computed by $Re = d_m \cdot u_m/\nu$ using the median equivalent bubble diameters, the kinematic viscosity $\nu = 10^{-6}\mathrm{m}^2/\mathrm{s}$ and the median bubble velocity measured at heights above the syringe of $> 10d_m$, assuming that the bubbles have reached their terminal velocity, as will be shown below. It could be seen, that the Reynolds number i.e. the rise velocity increases rapidly with increasing bubble spacing (lower bubble frequency), reaching its maximum at $L^* \approx 8$, which is a strong argument for bubble interaction in the form of hindrance as described for example by Ruzicka (2000), after that decaying slightly to $Re = 352$ for bubble spacings $L^* = 12$, which might be subject to shielding effects. However, the difference in Re is only about 10 and given the fact, that also the bubble size reduces slightly with increasing frequency the difference in Re is not distinct.

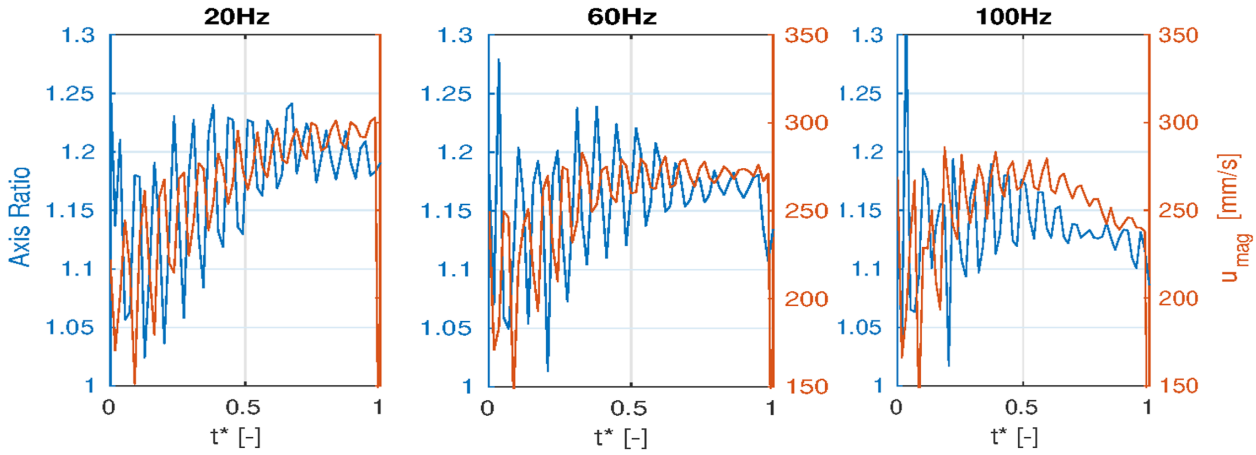

Figure 7: Axis Ratio oscillation vs. Velocity oscillation during acceleration period

Figure 7 shows the velocity and shape oscillation of exemplary bubbles, taken from the different frequency data sets. The dominant oscillation frequencies have been found to be at roughly 20 Hz regardless of the bubble frequency. Therefore it is assumed that the shape oscillations are predominantly subject to the bubble pinch-off process. During the pinch-off of the bubble the bubble-neck separates from the syringe and flips into the bubble resulting in an attenuated vertical oscillation of the bubble shape. This is also reflected in the bubbles magnitude velocity, which is also oscillating at the same frequency with a phase angle of roughly $\pi/2$.

Figure 8(a) - 8(e) shows exemplary PIV results of the time resolved measurements for bubble frequencies from $20 - 100$ Hz, the velocity magnitude is encoded by the background color. There are certain distinct features which develop with increasing bubble frequency. The most striking feature within the flow scenes is an area of high upwards directed velocity magnitude (see figure 8(d)) which develops with increasing bubbling frequency. This structure is similar to the vortex stucture, which was also observed by Sanada et al. (2005) and referred to as "Liquid Jet". This large scale vortical structure is fed by the liquid that is initially entrained by the bubbles directly after their formation. The emergence of this structure, which seems to have its center above the syringe tip also triggers the spreading of the bubble trajectories (see figure 9(a) - 9(c)). For low bubble frequencies the trajectories are nearly identical, the bubbles seem to enter the hull of the vortex structure at roughly the same position and seem to follow it with the same direction of rotation (most certainly counter-clock-wise). Starting at 60 Hz single bubbles leave the chain structure probably travelling in a counter clockwise spiral upwardly. The second striking tendency is the increasing velocity within the vertical spacing of the bubbles, indicating stronger bubble interaction, which is also reflected in the disappearing reproducibility of the bubble trajectories with increasing frequency (see fig. 9(a) - 9(c)). The authors believe that these accelerated volumes of liquid, together with the shape oscillations are the main influences on bubble chain dynamics, exerting forces such as, drag, lift forces, added mass and also Basset forces. Despite the undoubtedly three dimensional nature of the chain dynamics and the surrounding flow the present data might be used to calculate the acting forces on bubbles and aid the development of new approaches to the modelling of chain dynamics.

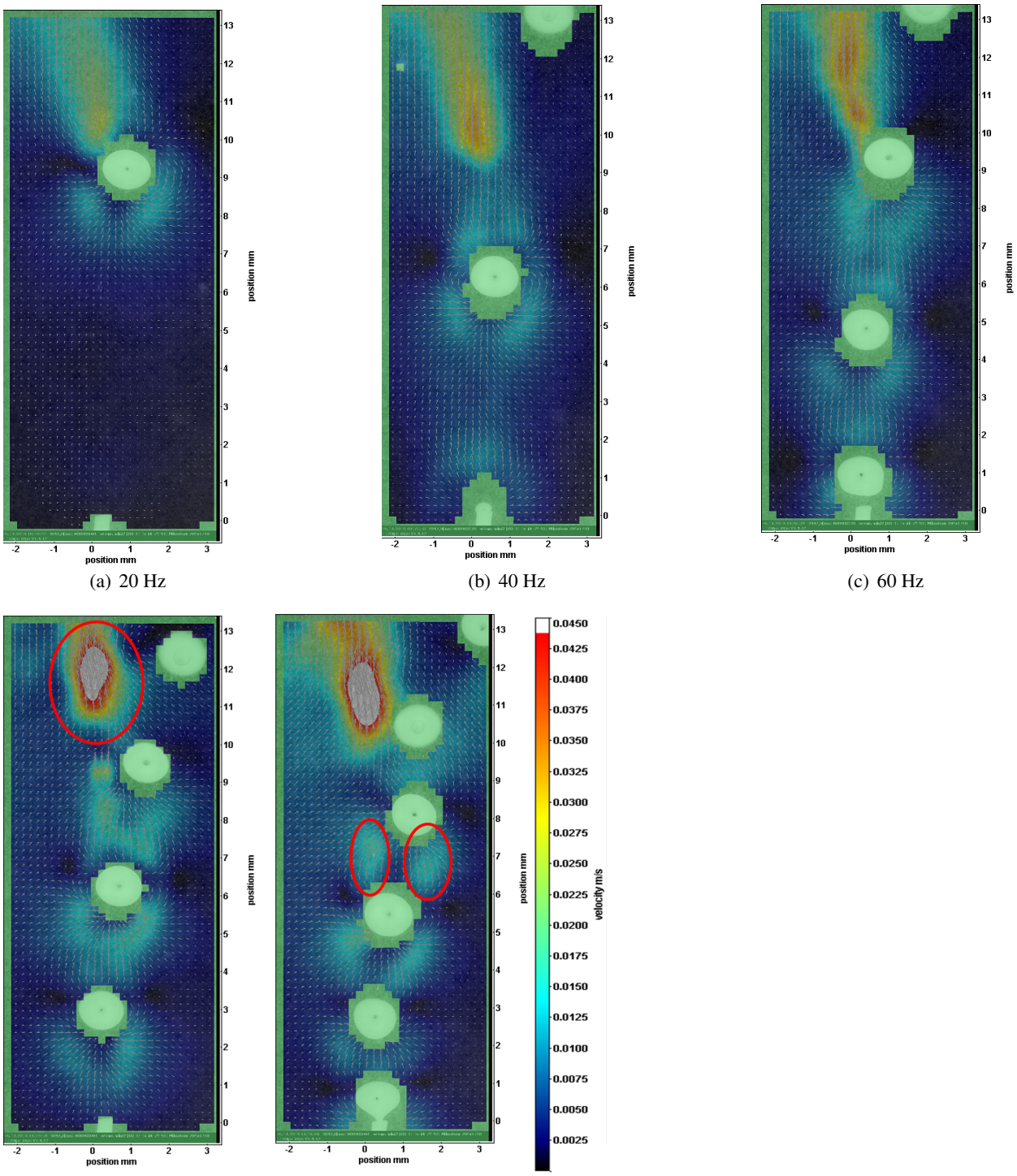

(a) 20 Hz (b) 40 Hz (c) 60 Hz

(d) 80 Hz (e) 100 Hz

Figure 8: Instantaneous velocity field for different bubbling frequencies

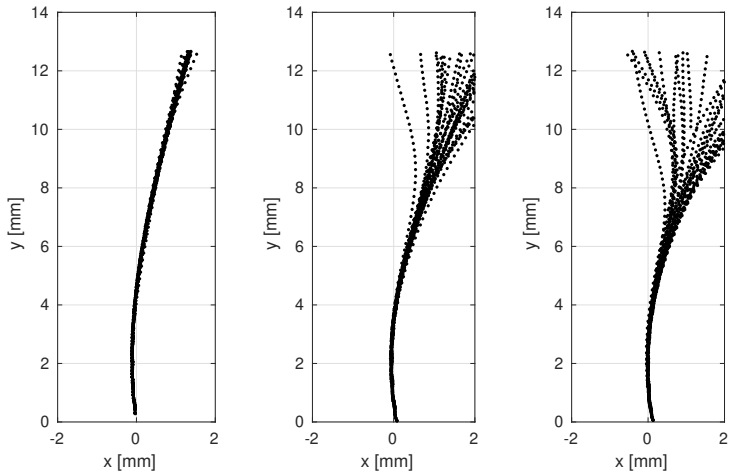

(a) 20 Hz (b) 60 Hz (c) 100 Hz

Figure 9: Particle Trajectories (n=30) at different bubble frequencies

4 Conclusion

The study reports on experiments on mono dispersed air bubble chains of diameters around 1.15 mm produced in water at varying frequencies from $20-100$ Hz. The flow field were measured using a shadography setup and standard 2D PIV. Furthermore, the bubbles were were traced analysed according to their shape, position. It is shown that the free stream bubble Reynolds number is effected by the parameter of the dimensionless bubble distance L^* and is decreasing with increasing bubble frequency, which is a strong indication for bubble-bubble interaction in the form of hindrance. Furthermore, it has been shown that the bubble shapes exhibit a strong vertical shape oscillation which also effects the magnitude of the bubble rising velocity at a phase shift of $\pi/2$. In addition the analysed bubbles always rise in line for a short period of $6-7$ bubble diameters. After that period of coherent chain formation horizontal dispersion occurs, also increasing with the bubble frequency. This effect is probably connected to a large scale coherent vortical structure which forms due to the entrained liquid. This structure is also referred as "Liquid Jet". However the measurements do not reflect the three dimensional nature of the flow and therefore only reflect a qualitative overview on the dynamics of bubble chains.

References

Elghobashi S (2019) Direct numerical simulation of turbulent flows laden with droplets or bubbles. *Annual Review of Fluid Mechanics* 51:217–244

Ostmann S and Schwarze R (2018) A compact device for the deterministic generation of medium-sized bubbles. *Review of Scientific Instruments* 89:125108

Ruzicka MC (2000) On bubbles rising in line. *International Journal of Multiphase Flow* 26:1141–1181

Sanada T, Watanabe M, Fukano T, and Kariyasaki A (2005) Behavior of a single coherent gas bubble chain and surrounding liquid jet flow structure. *Chemical Engineering Science* 60:4886–4900

Sommerfeld M and Bröder D (2009) Analysis of hydrodynamics and microstructure in a bubble column by planar shadow image velocimetry. *Industrial & Engineering Chemistry Research* 48:330–340

Vejrazka J, Fujasova M, Stanovsky P, Ruzicka MC, and Drahos J (2008) Bubbling controlled by needle movement. *Fluid Dynamics Research* 40:521